Journal Name

ARTICLE

Bio-inspired synthetic approaches: From hierarchical, hybrid supramolecular assemblies to $CaCO_3$-based microspheres

Received 00th January 20xx,
Accepted 00th January 20xx

DOI: 10.1039/x0xx00000x

www.rsc.org/

Bartosz Marzec,[a] Lei Zhang,[a,b] Nianyong Zhu[a,c] and Wolfgang Schmitt*[,a]

A bio-inspired synthetic approach to unprecedented hybrid supramolecular assemblies $[Ca(Me_2hda)(H_2O)_3]\cdot\frac{1}{2}MeOH\cdot\frac{1}{2}H_2O$ (**1**) and $[Ca(C_{12}hda)(H_2O)_2]\cdot H_2O$ (**2**), that are stabilized by iminodiacetate-substituted organic ligands is reported. The results of the single-crystal X-ray analysis of **1** further allowed the use of electron microscopy to verify the supramolecular structure of the fibrous assemblies of **2** that incorporate extended alkyl-substituted ligand derivatives. **2** reveals interesting features that distinguish these soft structures from purely inorganic, brittle materials: meshes of nanobelts transform on solid supports to form homogeneous films covering extended, micro-sized areas. The use of the reported ligand system as habit modifier for $CaCO_3$ results in hierarchical calcite aggregates. The structure-influencing effects of the ligands and their supramolecular assemblies promote the formation of calcite disks that tessellate into hollow microspheres that contain distinctive openings.

Introduction

Minerals of biological origin and their hybrid organic-inorganic composites often display complex, hierarchical organization of structure.[1] Sea urchin spines, coccoliths, bones, teeth and shells are the products of sophisticated synthetic methodologies where genetically-controlled and evolution-refined mineral deposition processes result locally in amorphous, poly- or single-crystalline phases.[2] Nature's remarkable ability to utilize such poorly processable inorganic materials to create biominerals characterised with impressive mechanical properties provides inspiration and motivation for materials scientists.[3] All biological mineral depositions involve self-organized organic macromolecules including proteins and polysaccharides imparting selectivity and specificity to biomineralisation processes.[4] The interactions between the organic matrixes and the mineralizing components are highly complex and require an appropriate geometry, stereochemistry and charge, establishing sites of nucleation and growth whereby predominantly donor atoms of alcohol, amine and carboxylate functionalities inhibit crystal faces, determining the growth directions and shapes of the minerals.[5-9]

Biological, affinity-driven aggregation of pre-organized molecules that characterise the initial steps of the formation of biominerals gives rise to the formation of hybrid organic-inorganic materials and are comparable to supramolecular self-assembly processes which are also developing into a key process in chemistry and material design.[10,11] Self-assembly processes that give rise to ordered structures generally rely on structural dynamics whereby individual entities either equilibrate between aggregated and non-aggregated states, or adjust their positions relative to one another once the ordered aggregate has formed.[12-15] In such systems the local environment generally influences prevailing inter-component forces whereby lateral boundaries and other possible templates impart directing effects and reduce possible defects.[16] Theoretical calculations reported by Goetz *et* al. underline that the amphiphilicity of self-assembling molecules is one crucial parameter that determines the structure and properties of the resulting products whereby small amphiphilic molecules or short polymers were proven to generate membrane-like assemblies in aqueous solutions.[17] The low bond energies of the interatomic forces that drive supramolecular assemblies to the thermodynamically most stable arrangements can give rise to reversibility and error checking/correction.[18]

Our research activities focus on the usage of bio-inspired, structurally well-characterised supramolecular coordination assemblies that self-organize into hierarchical hybrid nanomaterials. Our approach takes advantage of the ability to

[a] School of Chemistry & CRANN, University of Dublin, Trinity College, Dublin 2, Ireland. E-mail: schmittw@tcd.ie; Fax: +353-1-6712826; Tel: +353-1-8963495
[b] State Key Laboratory of Structural Chemistry, Fujian Institute of Research on the Structure of Matter, Chinese Academy of Sciences, Fuzhou, Fujian 350002, P. R. China;
[c] Institute of Molecular Functional Materials & Department of Chemistry, Hong Kong Baptist University, Waterloo Road, Hong Kong, HK; Supplementary Information (ESI) available: Full experimental procedures and Crystallographic data in CIF format for the new structure. See DOI: 10.1039/x0xx00000x

synthesize hydrogen-bonded or counter-ion mediated networks that are based on a modular set of aromatic iminodiacetic acid ligands (Fig. 1a). We previously demonstrated using transition metal complexes that the resulting supramolecular architectures are controlled by the substituents of these *hda* (2,2'-(2-hydroxybenzylazanediyl)diacetic acid) ligands producing lamellar structures, hexagonal assemblies or open-framework materials.[19-21] Many of the structures show resemblance to biological systems *e.g.* bi-layer membranes.[22] In related experiments we succeeded in producing highly aligned Na_2CO_3 containing nanofibres that are contained in carbon micro-containers which form upon thermolysis within a single crystal of a coordination network containing the starting components for the mineralization in a pre-arranged form;[23] some of the investigated transition metal complexes have the ability incorporate carbonate ligands that form upon fixation of atmospheric CO_2.[24]

The presented study explores the role of the *hda* ligand system on the formation of supramolecular Ca-based coordination assemblies and its influence as a habit modifier for the bio-inspired preparation of crystalline $CaCO_3$ materials. We present a coordination chemistry approach to habit modification whereby the amphiphilicity of the organic ligand systems was expected to influence supramolecular aggregation in solution, potentially resulting in confinement of the reaction volume. Thus the presented approach relates to biological templates that display various degrees of organization of structure. Whilst supramolecular coordination assemblies and network structures of transition metal ions that benefit from the ligand field stabilization are well-established,[25-30] the chemistry of related Ca^{2+} species remains underrepresented and less explored.[31-34] The here reported study provides insights into the coordination chemistry of these biologically important main-group systems. Structural information was obtained using a combination of electron microscopy, single-crystal and powder X-ray diffraction experiments.

Results and discussion

Ca^{2+} Binding Characteristics and Supramolecular Organization of the Selected Class of Organic Ligands

In order to obtain detailed structural information on the binding mode on a molecular level, we reacted the tetradentate dimethyl-substituted *hda* ligand (Me_2hda) with $CaCl_2$ in a MeOH/H_2O mixture to synthesize the novel compound $[Ca(Me_2hda)(H_2O)_3]\cdot½MeOH\cdot½H_2O$ (**1**), which separated phase-pure from the reaction mixture as colourless needle-shaped crystals. Single crystal X-ray analysis revealed that the species is composed of mononuclear secondary building units (Fig. 1b). The Ca^{2+} ions are surrounded by the six closest donor atoms in a highly unsymmetrical octahedral arrangement. Three water ligands adopt a *facial* arrangement and the inner coordination environment is completed by two *cis* coordinating O-donors that originate from deprotonated

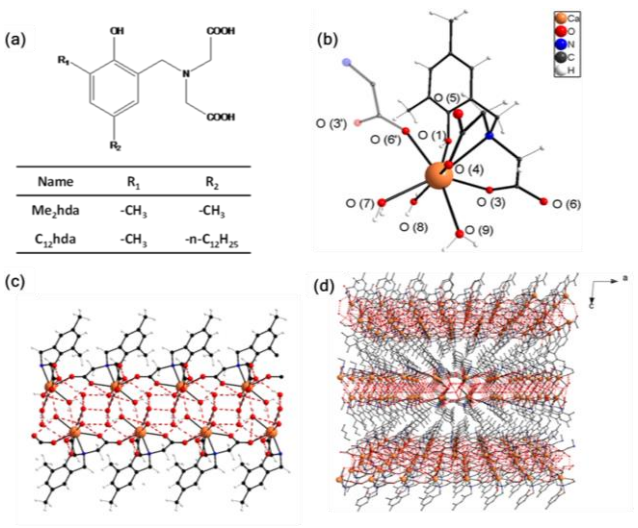

Fig. 1. (a) *Hda*-type ligands used in the present study. (b) Structure of the mononuclear secondary building unit in **1**. (c) Mononuclear building units are linked through coordination and hydrogen bonds to produce neutral layers extending in the crystallographic *ab*-plane. (d) Neutral layers aggregate through van der Waals forces to produce a layered, lamellar arrangement within the crystal structure of **1**; perspective view in the direction of the crystallographic [001]-axis.

carboxylic acid functionalities of a Me_2hda ligand and a symmetry generated O-donor, from a carboxylate function of a neighbouring secondary building unit, to give 1D chains that extend parallel to the crystallographic *a*-axis. The N-donor of the amine function and the O-donor of the protonated phenolic alcohol function of the Me_2hda ligand can be considered as a part of the outer coordination environment of the Ca^{2+} ion to give a very unsymmetrical 8-coordinated polyhedron. The amphiphilic character of the complexes promotes the formation of a layered lamellar supramolecular structure in which hydrophobic organic and hydrophilic inorganic layers are separated. Hydrogen bonds which involve the water ligands, the constitutional methanol and water molecules, the phenolic OH function and carboxylate O-donors link the chains within the *ab*-plane to form neutral layers (Figures 1c and d). The hydrogen bonds in 1 range between 2.219(2) Å and 2.933(2) Å, stabilizing neutral layers with a cross-sectional thickness of *ca.* 1.7 nm. These layers interact through dispersion forces with each other and pack in the *c*-direction to form a layered lamellar structure. The layered, amphiphilic nature of **1** combined with the observed anisotropic growth directions within a neutral layer gives rise to the formation of 1D or 2D crystal and assembly morphologies. In fact, crystalline microfibres of **1** whose dimensions are characterised by high aspect ratios (millimeter lengths and diameters of *ca*. 700 nm) can be grown upon slight variation of the preparation conditions.

Isolated metal complexes with three facial water molecules are relatively rarely observed since vacant H_2O ligand sites often promote hydrolytic condensations, dimerization or oligomerizations.[35] The observed type of complex is generally regarded to impose directionality in condensation reactions whereby the complex can provide a capping unit that stabilises

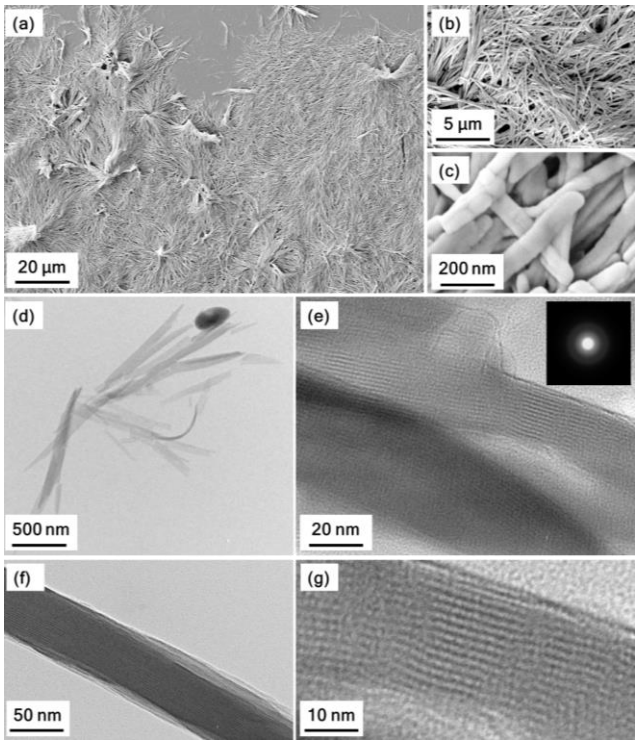

Fig. 2. (a-c) SEM images of the assemblies of **2** confirm their fibrous morphology. (d-g) HR-TEM images reveal that **2** has a layered lamellar structure, where the separation distance between the interference fringes is *ca.* 2.5 nm. The inset shows electron diffraction image recorded for a single fiber and confirms that **2** is initially an amorphous material.

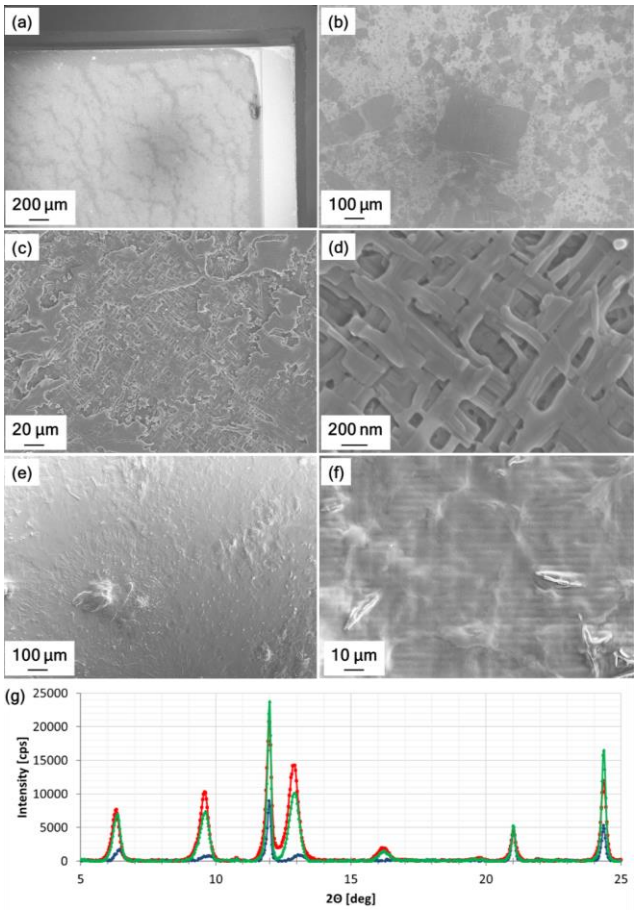

Fig. 3. SEM images recorded for a sample of **2** deposited on a Si substrate after two weeks (a-d) and four weeks (e-f) show the morphological transition from a cross-bar type motif to a smooth film. (g) Powder-X-ray diffraction patterns of assemblies of **2** recorded over a time period of two weeks; (the sample was deposited on a low background Si stub) - (blue) fresh sample; (green) one week after preparation; (red) two weeks after preparation.

portions of condensing mineral structures. The three water molecules provide distinct binding sites for chelating moieties, in particular for carbonate and hydrogen carbonate ions. In this context one of the most remarkable, partially hydrated main-group binding sites in nature is represented in ribulose-1,5-bisphosphate (RuBP) carboxylase, whose Mg^{2+} site initiates the first step in photosynthetic CO_2 fixation providing carbamate binding sites.[36] Depending on the pH of a given reaction system, metal-bound aqua ligands undergo deprotonation to form hydroxo moieties that can act as nucleophiles, *e.g.* in the presence of CO_2, promoting its conversion to carbonate and hydrogen carbonate in d^{10} Zn-containing carbonic anhydrases.[37]

Influencing the amphiphilicity of the Ca-complexes – Towards functional, soft, hierarchical nanomaterials

The nature of the ligand substituents in the *ortho* and *para* positions with respect to the phenolic OH-functionality provides a synthetic parameter to control the amphiphilicity to exploit the described type of compounds for self-assembly purposes and to generate hierarchical soft materials. Increasing the hydrophobicity of the *hda* ligand and introducing *n*-C_{12}-alkyl chain in the *para* position (Fig. 1) influences the morphology of the obtained self-assembled materials. The species $[Ca(C_{12}hda)(H_2O)_2]\cdot H_2O$ (**2**) forms when calcium chloride is reacted with the C_{12}hda ligand under similar conditions to those that led to the formation of **1**. **2** rapidly precipitates from the solution producing fibrous assemblies with high aspect ratios. The constitution of **2** was substantiated by CHN analysis, EDX spectroscopy and thermogravimetric analysis (see ESI). Differences between **1** and **2** in the thermal degradation pathway in an air atmosphere mainly derive from the presence of different quantities of coordinating solvent molecules and the length of the alkyl moieties of the organic ligands. The degradation of the organic ligands occurs above *ca.* 200 °C initially resulting in the formation of $CaCO_3$ then forming CaO at further elevated temperatures. A comparison of the IR spectra of **1** and **2** (ESI, Fig. S3) indicates that signals attributable to the asymmetric and symmetric vibrations of the carboxylate functionalities of the organic ligands, display similar shifts. The relative differences $\Delta\nu = \nu_a - \nu_s$ agree with the observed binding mode in **1**. Thus, this observation supports the assumption that C_{12}Mehda and Me_2hda bind to Ca^{2+} ions in a similar fashion and resulting in comparable coordination environments. Electron micrographs (Figs. 2a-c) confirm that a typical sample contains belt-like assemblies of sub-millimeter lengths whose thickness and widths vary between 30-50 nm and 80-300 nm, respectively. HR-TEM analysis (Figs. 2d-f) confirms that the layered lamellar supramolecular structure is preserved in the assemblies. Neutral layers extend parallel to the

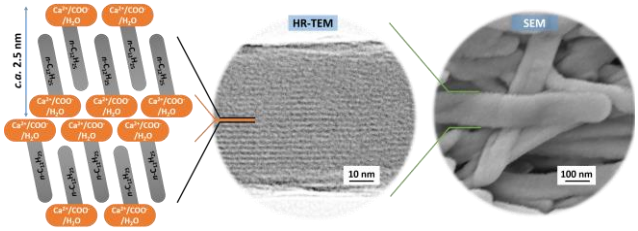

Fig. 4. Scheme highlighting the relationship between molecular and microscopic structure in **2**.

longest and shortest belt axes and stack across the width of the belt with a separation distance of *ca.* 2.5 ± 0.2 nm (Fig. 2g) which is very well in agreement with the extent of the alkyl moieties of the organic ligands. The electron diffraction pattern shows no evidence of further ordering within the compound (*inset* Fig. 2e).

The soft, flexible nature distinguishes these hierarchical bio-inspired assemblies of **2** from brittle crystalline materials. We noticed that the fibrous structures in as-prepared solid samples are capable of undergoing structural rearrangements at room temperature. When the sample is left for two weeks on a SiO_2 surface, extended film areas (max. observed dimension 0.3 mm x 0.5 mm) appear to form (Figs. 3a-b). We noticed that this morphological rearrangement seemed to involve the formation of crossbar or grid motifs whereby single belts are crossed in an ordered fashion (Figs. 3c-d). After four weeks from the preparation, meshes of entangled belts amalgam to produce homogenous, continuous films that extend over the surface of the sample (Figs. 3e-f). Overview SEM images at intermediate stages further reveal distinct areas of film formation; often almost rectangular, 2D crystalline patches with micrometre dimensions appear at various places on the surfaces. As the time progresses some of these patches further develop into larger extended areas.

To further investigate the nature of the observed transformations, we compared FT-IR and Raman spectra of **2** as well as the corresponding powder X-ray diffraction (P-XRD) patterns of freshly precipitated samples and samples that were one and two weeks old. No significant shifts in IR or Raman spectra occurred over the examined time period, strongly suggesting that the composition and molecular structure of the samples remains largely unchanged during the rearrangement and the film formation. The recorded time-dependent P-XRD patterns revealed that although the freshly precipitated fibres of **2** were initially amorphous or poorly crystalline, the material rearranged within the first week to give a more ordered crystalline phase. During this investigated time period, one observes the development of a series of reflections in the lower 2Θ range at 6.31°, 9.58°, 12.88° and 16.15°, which can be attributed to the stacking distance between neutral layers in 2 (for n = 2, 3, 4 and 5, respectively, cording to the Bragg equation, Figure 3g). The lattice separation distance calculated for these 2Θ values equals 2.79 nm and is in agreement with the distance between the interference fringes observed in HR-TEM images (Figure 2g, ~2.5 nm). Reflections related to the lattice parameter that corresponds to the thickness of the film appear as rather weak, broad signals.

The initially deposited entangled fibrous material of **2** may be regarded as a metastable assembly at a lateral boundary,[38] which is prone to structural rearrangements on time-scales that are influenced by the chemical environment and the nature of involved chemical bonds whereby transformation to the equilibrium state is characterised by coarsening effects, *e.g.* a dimensional expansion of a characteristic dominant structure. The observed morphological change did not occur in samples that were fully dried or fully dehydrated after the preparation (by treatment at elevated temperatures or keeping the samples under vacuum). This observation suggests that the driving force of the rearrangement is associated with the evaporation/re-location of solvent molecules and H-bonds, which occurs when a sample is left in ambient conditions. In aqueous environments the surface of the fibrous assemblies of **2** is composed mainly of water molecules. As direct consequence of the anisotropic morphology of the belt-like fibres, neutral layers in **2** arrange perpendicular with respect to the deposition surface – this arrangement appears to be a requirement for the observed coarsening effect to form extended films. A pictogram showing the HR-TEM imaging and highlighting the relationship between molecular and microscopic structure of **2** is presented in Figure 4. On the relatively hydrophilic SiO_2 surface, the layers may rearrange whereby hydrophilic parts of the structure are expected to preferentially interact with the substrate. Competing hydrogen bonds and electrostatic interactions that occur between the hydrophilic parts of the assemblies and van der Waals forces involving the organic residues, seemed responsible for the formation of a thin and smooth films, whereby larger domains seemed to grow at the expense of smaller domains (similar to Ostwald ripening effects). Thus, these underlying weak intermolecular forces in combination with the layered lamellar supramolecular structure of the material are responsible for fibrous assemblies that are in contact to each other to amalgam and rearrange to form continuous, homogeneous firms.

The observed phenomenon that promotes the formation of homogenous, continuous films that extend over large areas may also apply to other structurally related materials with advantageous surface or electronic/optical properties, thus providing a future perspective of supramolecular approaches being exploited for biocompatible coatings or electronic/optical device fabrication.[39] The observed characteristics may also be of interest in the context of self-healing materials.[40] Further, soft fibrous materials with high aspect ratios that degrade into more stable and safe inorganic products (e.g. $CaCO_3$) are desired composite materials for regenerative medical purposes.[41]

Use of the ligand system as habit modifiers for $CaCO_3$

The crystallographic study of **1** provided us with a detailed molecular understanding of the complexing ability of the *hda* ligands. The partially 'open' Ca^{2+} environments that contain terminal H_2O sites which can be involved in hydrolytic condensations or which can provide strong binding affinity for additional chelating O-donor groups, suggests that this ligand-type could be an interesting class of habit modifier selectively inhibiting

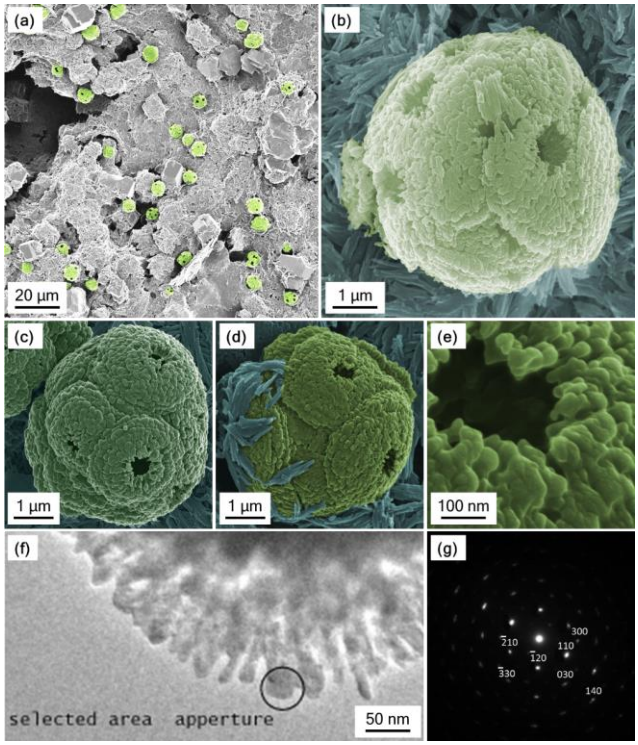

Fig. 5. (a-e) False color HeIM micrographs of microspherical $CaCO_3$ structures that assemble in the presence of C_{12}hda as the templating agent; (a) Overview of a usual sample. (b) Enlarged example of the discussed morphology. (c-e) Microspherical morphology. (f) TEM image on the edge of an individual calcite disk highlighting the position of the selected area aperture that was used to collect the corresponding electron diffraction pattern (g).

growth directions of specific $CaCO_3$ crystal faces. Moreover, the self-organization tendency to form **2** underlines the capability of the ligand system to generate highly ordered amphiphilic aggregates that can provide appropriate spatial periodicity to produce morphology-directing matrices or confinement effects. The glycine-type functionality of the chosen ligand system correlates biomimetically very well with the low isoelectric points of proteins that are typically involved in natural $CaCO_3$ mineralization and which contain primarily aspartate or glutamate residues.[42-45] Related previously reported studies to control and template calcifications have focused on structured organic surfaces including thin films and Langmuir monolayers;[46, 47] other studies use organic and inorganic additives,[48] synthetic polymers[49] and co-polymers[50] or extracted biopolymers.[51]

In consecutive experiments we increased the Ca^{2+}/C_{12}hda mole ratio in aqueous solutions up to 100:1 and induced $CaCO_3$ formation through addition of $NaHCO_3$. The reaction mixture was constantly agitated and during initial experiments the temperature of the reaction mixture was kept at 40°C. X-ray powder diffraction and IR spectroscopy confirm that above a Ca^{2+}/C_{12}hda ratio of 25:1, phase-pure calcite products separate from the reaction mixture. The phase identity of these crystallites was further confirmed in a TEM electron diffraction experiment, whereby the recorded diffraction pattern was indexed as calcite. At lower Ca^{2+}/C_{12}hda ratios the chelating ability of the ligand suppresses $CaCO_3$ precipitation and we observe the afore described fibrous assemblies of metal complex **2**. Preliminary tests clearly demonstrated that the ligand system distinctively perturbates the $CaCO_3$ mineralization at a Ca^{2+}/C_{12}hda ratio higher than 15:1 and below 50:1 and we focused our attention on exploring slight variations of experimental conditions in this concentration regime. Noteworthy in a Ca^{2+}/C_{12}hda range between 20:1–25:1 our SEM investigations revealed the formation of spherical structures (Figs. 5a-e). The spheres are created by aggregation of characteristic calcite discs. Each disk is composed of small nanosized particulates and has a hollow centre. The cross-sectional diameters of the disks typically vary between *ca*. 2-3 µm and the central openings are characterised by diameters that range between 400-800 nm. The entire spherical assembly has a diameter of *ca.* 8-12 µm and is typically built of 7-11 spherical disks producing a hollow microstructure with a wall thickness that does not exceed 1 µm. FT-IR and EDX spectroscopy including elemental mapping have confirmed that the structures are composed of calcium carbonate and powder X-ray diffraction revealed that calcite is the predominant phase.

TEM electron diffraction experiment confirmed that the individual disks assembling into the hollow sphere were composed of calcite (Figs. 5f-g). We speculate that the amphiphilicity of the ligand or of the resulting Ca^{2+} complexes promotes the formation of micellular or vesicular assemblies in water which provide morphology-directing matrices for the $CaCO_3$ mineralization. This assumption is substantiated by the observation of spherical assemblies of *hda* transition metal complexes that form under comparable reaction conditions.[20]

As expected, during the $CaCO_3$ precipitation at a Ca^{2+}/C_{12}hda ratio of 25:1 the initial pH of 6.9 increases to 8.3 within 24 h and then remained constant. X-ray powder diffraction experiments confirm that $CaCO_3$ precipitation initially produces amorphous phases (ACC) that age to yield coexisting phases of calcite and vaterite after 1 h; calcite phases containing sphere-like morphologies were obtained after 24 hours (Fig. 6a). We further investigated the formation conditions of this unexpected morphology and varied the initial temperature and pH range. While elevating the temperature above 60°C increased the solubility of the C_{12}hda ligand, it also resulted in the precipitation of aragonite needles (Fig. 6c), which is in agreement with the observations of Beck *et* al.[52] The described spherical morphologies predominantly form in a pH range between 6.9–8.3 between 30-40°C. Acidification of the reaction mixture, which was achieved through the addition of 0.2 M HCl, resulted either in the dissolution of the $CaCO_3$ precipitates below pH 6.5, or in the precipitation of morphologically related spheres which are shown in Fig. 6d. These form at an initial pH value of 6.5 (ESI, Table S1). Increasing the initial pH value above 8.0 through the addition of NaOH results in the precipitation of *ca*. 20 µm large, rhombohedral calcite crystals that contain residual amounts of **2** (Fig. 6e).

The observed spherical, bio-inspired morphologies morphologies of $CaCO_3$ reveal some vague resemblance to natural coccospheres which are produced by several species of marine algae, including *Emiliania huxleyi* and *Gephyrocapsa oceanica* and which represent a fascinating $CaCO_3$ biomaterials whose complex structural attributes are represented by the observed inherent chirality that is expressed

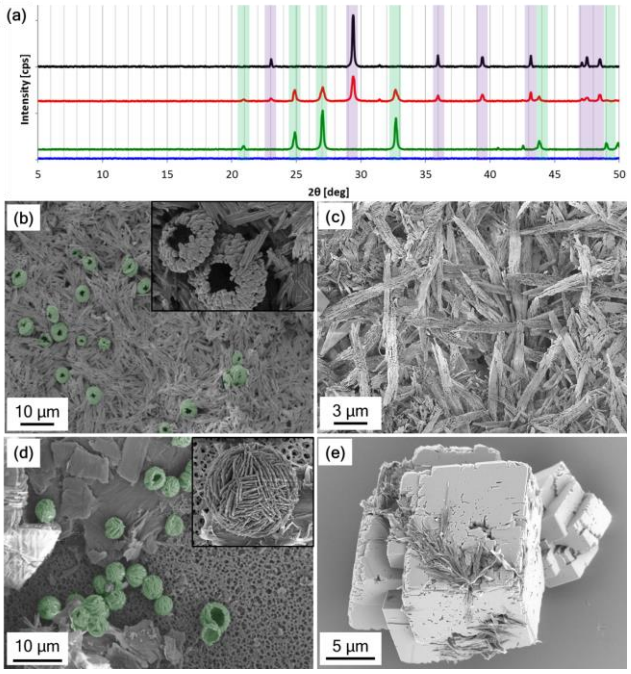

Fig. 6. (a) Powder X-ray diffraction patterns recorded for the precipitate forming in a 16.7 mM Ca^{2+} reaction crystallisation mixture (C_{12}hda/Ca^{2+}/HCO_3^- mole ratio 1:25:50, see ESI, Table S1); after 5 minutes (blue), 30 minutes (green), 60 minutes (red) and 24 hours (black). The highlighted areas show the typical positions of calcite (violet) and vaterite (green) reflections. (b) SEM image of individual calcite disks observed in the reaction mixture. (c) SEM image of needle-shaped aragonite crystals precipitated in the presence of C_{12}hda at temperatures higher than 60 °C. (d) SEM image of calcite spheres obtained upon acidification of the reaction system (see ESI, Table S1). (e) SEM image of a rhombohedral calcite crystal containing residual quntities of **2** that formed upon addition of NaOH (1 M) to the growth mixture (intitial pH above 8.0, ESI Fig. S15 (g & h)).

at several distinct scale levels.[53] It should be clearly stated that the natural formation of these species is not mechanistically related to the here applied formation processes of the observed spheres.

The formation of the observed spheres as shown in Fig. 5 may be rationalized by taking into account the composition of the reaction media and considering the initial formation of ACC. Based on literature examples two possible formation pathways may apply. One possibility involves the self-transformation of *hda*-stabilized solid ACC microspheres *via* surface-directed Ostwald ripening to form hollow calcite spheres. Considering this scenario, the observed surface patterning is the result of a CO_2 outgassing processes, thus, the formation relates to processes that were previously observed by Mann and co-workers.[54] A second possible formation mechanism may involve the aggregation of ACC/*hda* nanospheres at the underside of CO_2 droplets trapped in the meniscus at the air/water interface. This approach can explain the distinct curved shape of the disks. As the CO_2 templated bubble starts to sink, further discs are formed and tessellate the surface. The latter formation approach is supported by the observation that individual disks are indeed observed in the reaction system (see Fig. 6b); these can exist in significant quantities depending on the reaction temperature and thus are influenced by dynamic processes at the air/water interface.[55] The formation of the observed spheres may further involve the formation of transient vaterite spheres, which is a morphology often assumed by this particular polymorph.[56]

Conclusions

In conclusion, we report a bio-inspired synthetic approach that results in unprecedented hybrid supramolecular assemblies **1** and **2**, and $CaCO_3$ materials with micro-spherical morphologies. The crystal structure of **1** provided a detailed understanding of the supramolecular structure and binding mode of the involved donor atoms, providing clues on how *hda*-type ligands can be exploited as habit modifiers to template hierarchical $CaCO_3$ mineral structures. The results of the X-ray analysis of **1** further allowed us to use electron microscopy to verify the supramolecular structure of the fibrous assemblies of **2** that incorporate extended C_{12}hda ligands. The resulting soft, hybrid materials reveal interesting features that distinguish them from purely inorganic, brittle materials: meshes of nanobelts transform into highly ordered crossbar assemblies and homogeneous films whereby the mononuclear amphiphiles rearrange to produce extended, micro-sized areas. The observed phenomenon may in the future be applicable to self-healing films or regenerative medical purposes, thus providing a perspective of supramolecular approaches being applied in materials science. Soft fibrous materials with high aspect ratios that slowly degrade into calcium carbonate- or phosphate-containing hybrid materials are expected to enhance epitaxial bone or enamel regeneration in vivo.[57] The use of the reported ligand system as habit modifier for $CaCO_3$ results in hierarchical calcite aggregates. The structure-influencing effects of the ligands and their supramolecular assemblies promote the formation of micro-spherical calcite disks (most likely in the presence of CO_2 bubbles) that tessellate into hollow microspheres that contain distinctive openings.

Experimental

The *hda* ligands were prepared by Mannich reaction between the appropriate phenol, iminodiacetic acid and aqueous formaldehyde.[58]

1: 0.027 g (0.1 mmol) of Me_2hda was dissolved in a 1:1 (v/v) mixture of water and methanol under ambient conditions. Addition of 28 µL of triethylamine (0.215 mmol) and 50 µL of an aqueous $CaCl_2$ solution (1M) afforded the formation of crystals of 1 after seven days. Yield: 44%. Elemental analysis excepted for $C_{13}CaH_{21}NO_8$: (without crystallization solvent molecules): C: 43.45%, H: 5.89%, Ca: 11.15%, N: 3.90; Found: C: 42.92%, H: 5.97%, Ca: 10.81%, N: 3.69%. IR/cm^{-1} : 2923 (m), 2852 (m), 1586 (s), 1410 (m), 1325 (s), 1246 (s), 1221 (s), 1152 (s), 990 (s), 867 (s), 721 (m).

2: 0.042 g (0.10 mmol) of C_{12}hda was dissolved at 40ºC in a mixture of 3.5 ml of water and 6 mL of MeOH. Addition of 28 µL (0.2 mmol) of triethylamine and of 0.5 mL of an aqueous $CaCl_2$ solution (0.1M) caused the instant formation of a white precipitate of 2. Yield: 84%. Elemental analysis excepted for $C_{24}CaH_{43}NO_7$ (without free solvent molecules): C: 57.92%, H: 8.71%, Ca: 8.05%, N: 2.81%; Found: C: 58.27%, H: 8.15%, Ca: 8.10%, N: 2.83%. IR/cm^{-1} : 3853(vw), 3225(s, broad), 2918(s), 2848(s), 2368(vw), 1655(m), 1614(m), 1582(s),

1489(w), 1415(m), 1322(w), 1241(w), 1217(w), 988(w), 865(w), 721(m).

$CaCO_3$ precipitation experiments: $CaCO_3$ precipitates form upon addition of $CaCl_2$ to an aqueous solution of C_{12}hda and $NaHCO_3$ at specific temperatures. Detailed reactions conditions and analyses of the resulting $CaCO_3$ materials are provided in the Electronic Supplementary Information (see Table S1).

Crystallography: Details of data collection and refinement for **1** are given in the Supporting Information (Table S2). Crystallographic data, CCDC 793553, can be obtained free of charge from the Cambridge Crystallographic Data Centre via www.ccdc.cam.ac.uk/data_request /cif.

Acknowledgement

Financial Support from the Science Foundation Ireland (SFI; 06/RFP/CHE174 and 13/IA/1896), the European Research Council (CoG 2014 – 647719) and DRHEA (B.M.) is gratefully acknowledged.

Notes and references

1. P. Fratzl and R. Weinkamer, *Prog. Mater. Sci.*, 2007, **52**, 1263-1334.
2. M. A. Meyers, P.-Y. Chen, A. Y.-M. Lin and Y. Seki, *Prog. Mater. Sci.*, 2007, **53**, 1-206.
3. W. Kunz and M. Kellermeier, *Science*, 2009, **323**, 344-345.
4. A. Arakaki, K. Shimizu, M. Oda, T. Sakamoto, T. Nishimura and T. Kato, *Org. Biomol. Chem.*, 2015, **13**, 974-989.
5. L. Addadi and S. Weiner, *Nature*, 2001, **411**, 753, 755.
6. E. Beniash, J. P. Simmer and H. C. Margolis, *J. Struct. Biol.*, 2005, **149**, 182-190.
7. H. Shiraga, W. Min, W. J. VanDusen, M. D. Clayman, D. Miner, C. H. Terrell, J. R. Sherbotie, J. W. Foreman, C. Przysiecki and a. et, *Proc. Natl. Acad. Sci. U. S. A.*, 1992, **89**, 426-430.
8. M. Okaniwa, Y. Oaki and H. Imai, *Bull. Chem. Soc. Jpn.*, 2015, **88**(*10*), 1459-1456.
9. K. Ariga, K. Kawakami, M. Ebara, Y. Kotsuchibashi, Q. Ji and J. P. Hill, *New J. Chem.*, 2014, **38**, 5149-5163.
10. J. F. Banfield, S. A. Welch, H. Zhang, T. T. Ebert and R. L. Penn, *Science*, 2000, **289**, 751-754.
11. A.-W. Xu, M. Antonietti, H. Coelfen and Y.-P. Fang, *Adv. Funct. Mater.*, 2006, **16**, 903-908.
12. P. Yin, H. M. T. Choi, C. R. Calvert and N. A. Pierce, *Nature*, 2008, **451**, 318-322.
13. M. Yoshitake, K. Kubo, T. Endo, S.-I. Noro, T. Akutagawa and T. Nakamura, *Bull. Chem. Soc. Jpn.*, 2016, **89**, 354-360.
14. W. Wang, Y.-X. Wang and H.-B. Yang, *Chem. Soc. Rev.*, 2016, **45**, 2656-2693.
15. N. Yoshinari, A. Kakuya, R. Lee and T. Konno, *Bull. Chem. Soc. Jpn.*, 2015, 88, 59-68.
16. P. A. Korevaar, C. Schaefer, T. F. A. de Greef and E. W. Meijer, *J. Am. Chem. Soc.*, 2012, **134**, 13482-13491.
17. R. Goetz, G. Gompper and R. Lipowsky, *Phys. Rev. Lett.*, 1999, **82**, 221-224.
18. W. Jiang, A. Schaefer, P. C. Mohr and C. A. Schalley, *J. Am. Chem. Soc.*, 2010, **132**, 2309-2320.
19. G. La Spina, R. Clérac, E. S. Collins, T. McCabe, M. Venkatesan, I. Ichinose and W. Schmitt, *Dalton Trans.*, 2007, 5248-5252.
20. I. McKeogh, J. P. Hill, E. S. Collins, T. McCabe, A. K. Powell and W. Schmitt, *New J. Chem.*, 2007, **31**, 1882-1886.
21. W. Schmitt, J. P. Hill, M. P. Juanico, A. Caneschi, F. Costantino, C. E. Anson and A. K. Powell, *Angew. Chem. Int. Ed.*, 2005, **44**, 4187-4192.
22. R. Timpl and J. C. Brown, *BioEssays*, 1996, **18**, 123-132.
23. W. Schmitt, J. P. Hill, S. Malik, C. A. Volkert, I. Ichinose, C. E. Anson and A. K. Powell, *Angew. Chem. Int. Ed.*, 2005, **44**, 7048-7053.
24. WO2013072906A2, 2013.
25. A. J. Blake, N. R. Champness, P. Hubberstey, W.-S. Li, M. A. Withersby and M. Schröder, *Coord. Chem. Rev.*, 1999, **183**, 117-138.
26. H. Abourahma, G. J. Bodwell, J. Lu, B. Moulton, I. R. Pottie, R. Bailey Walsh and M. J. Zaworotko, *Cryst. Growth Des.*, 2003, **3**, 513-519.
27. T. Fujigaya, D.-L. Jiang and T. Aida, *J. Am. Chem. Soc.*, 2003, **125**, 14690-14691.
28. V. W.-W. Yam, K. K.-W. Lo, C.-R. Wang and K.-K. Cheung, *J. Phys. Chem. A*, 1997, **101**, 4666-4672.
29. A. M. Ako, M. S. Alam, M. Rahman, J. P. Hill, N. M. Sanchez-Ballester, K. Ariga, G. Buth, C. E. Anson and A. K. Powell, *Chem. - Eur. J.*, 2012, **18**, 16419-16425.
30. N. M. Sanchez-Ballester, L. K. Shrestha, M. R. J. Elsegood, W. Schmitt, K. Ariga, C. E. Anson, J. P. Hill and A. K. Powell, *Dalton Trans.*, 2013, **42**, 2779-2785.
31. Y. Sun, Y. Sun, H. Zheng, H. Wang, Y. Han, Y. Yang and L. Wang, *CrystEngComm*, 2016, **18**, 8664-8671.
32. S. Kobayashi and Y. Yamashita, *Acc. Chem. Res.*, 2011, **44**, 58-71.
33. M. Albrecht, Y. Liu, S. S. Zhu, C. A. Schalley and R. Fröhlich, *Chem. Commun.*, 2009, 1195-1197.
34. S.-I. Noro, J. Mizutani, Y. Hijikata, R. Matsuda, H. Sato, S. Kitagawa, K. Sugimoto, Y. Inubushi, K. Kubo and T. Nakamura, *Nat. Commun.*, 2015, **6**, 5851.
35. D. Hoebbel, T. Reinert, H. Schmidt and E. Arpac, *J. Sol-Gel Sci. Technol.*, 1997, **10**, 115-126.
36. R. J. Spreitzer and M. E. Salvucci, *Annu. Rev. Plant Biol.*, 2002, **53**, 449-475.
37. M. G. Lionetto, R. Caricato, M. E. Giordano and T. Schettino, *Int. J. Mol. Sci.*, 2016, **17**, 127/121-127/114.
38. D. J. Adams, K. Morris, L. Chen, L. C. Serpell, J. Bacsa and G. M. Day, *Soft Matter*, 2010, **6**, 4144-4156.
39. V. Stavila, A. A. Talin and M. D. Allendorf, *Chem. Soc. Rev.*, 2014, **43**(*16*), 5994-6010.
40. R. P. Wool, *Soft Matter*, 2008, **4**, 400-418.
41. S. I. Stupp, *Nano Lett.*, 2010, **10**(*12*), 4783-4786.
42. X. Gan, K. He, B. Qian, Q. Deng, L. Lu and Y. Wang, *J. Cryst. Growth*, 2017, **458**, 60-65.
43. B.-A. Gotliv, L. Addadi and S. Weiner, *ChemBioChem*, 2003, **4**, 522-529.
44. Y. Politi, J. Mahamid, H. Goldberg, S. Weiner and L. Addadi, *CrystEngComm*, 2007, **9**, 1171-1177.
45. S. E. Wolf, J. Leiterer, V. Pipich, R. Barrea, F. Emmerling and W. Tremel, *J. Am. Chem. Soc.*, 2011, **133**, 12642-12649.
46. B. R. Heywood and S. Mann, *Chem. Mater.*, 1994, **6**, 311-318.
47. E. Loste, E. Diaz-Marti, A. Zarbakhsh and F. C. Meldrum, *Langmuir*, 2003, **19**, 2830-2837.
48. D. Gebauer, H. Coelfen, A. Verch and M. Antonietti, *Adv. Mater.*, 2009, **21**, 435-439.
49. B. Cantaert, Y.-Y. Kim, H. Ludwig, F. Nudelman, N. A. J. M. Sommerdijk and F. C. Meldrum, *Adv. Funct. Mater.*, 2012, **22**, 907-915.
50. A. S. Schenk, H. Zope, Y.-Y. Kim, A. Kros, N. A. J. M. Sommerdijk and F. C. Meldrum, *Faraday Discuss.*, 2012, **159**, 327-344.
51. A. Gal, K. Kahil, N. Vidavsky, R. T. DeVol, P. U. P. A. Gilbert, P. Fratzl, S. Weiner and L. Addadi, *Adv. Funct. Mater.*, 2014, **24**, 5420-5426.
52. R. Beck and J.-P. Andreassen, *J. Cryst. Growth*, 2010, **312**, 2226-2238.
53. P. Westbroek, E. W. De Jong, P. Van der Wal, A. H. Borman, J. P. M. De Vrind, D. Kok, W. C. De Bruijn and S. B. Parker, *Philos. Trans. R. Soc. London, Ser. B*, 1984, **304**, 435-444, 431 plate.
54. J. G. Yu, H. Guo, S. A. Davis and S. Mann, *Adv. Funct. Mater.*, 2006, **16**, 2035-2041.
55. J. Rudloff and H. Coelfen, *Langmuir*, 2004, **20**, 991-996.
56. J.-P. Andreassen, *J. Cryst. Growth*, 2005, **274**, 256-264.
57. Z. A. C. Schnepp, R. Gonzalez-McQuire and S. Mann, *Adv. Mater.*, 2006, **18**, 1869-1872.

58. V. Y. Temkina, M. N. Rusina, G. F. Yaroshenko, M. Z. Branzburg, L. M. Timakova and N. M. Dyatlova, *Zhurnal Obshchei Khimii*, 1975, **45**, 1564-1570.

Graphical Abstract: